FINAL REPORT

for

VENUS WIND-ALTITUDE RADAR

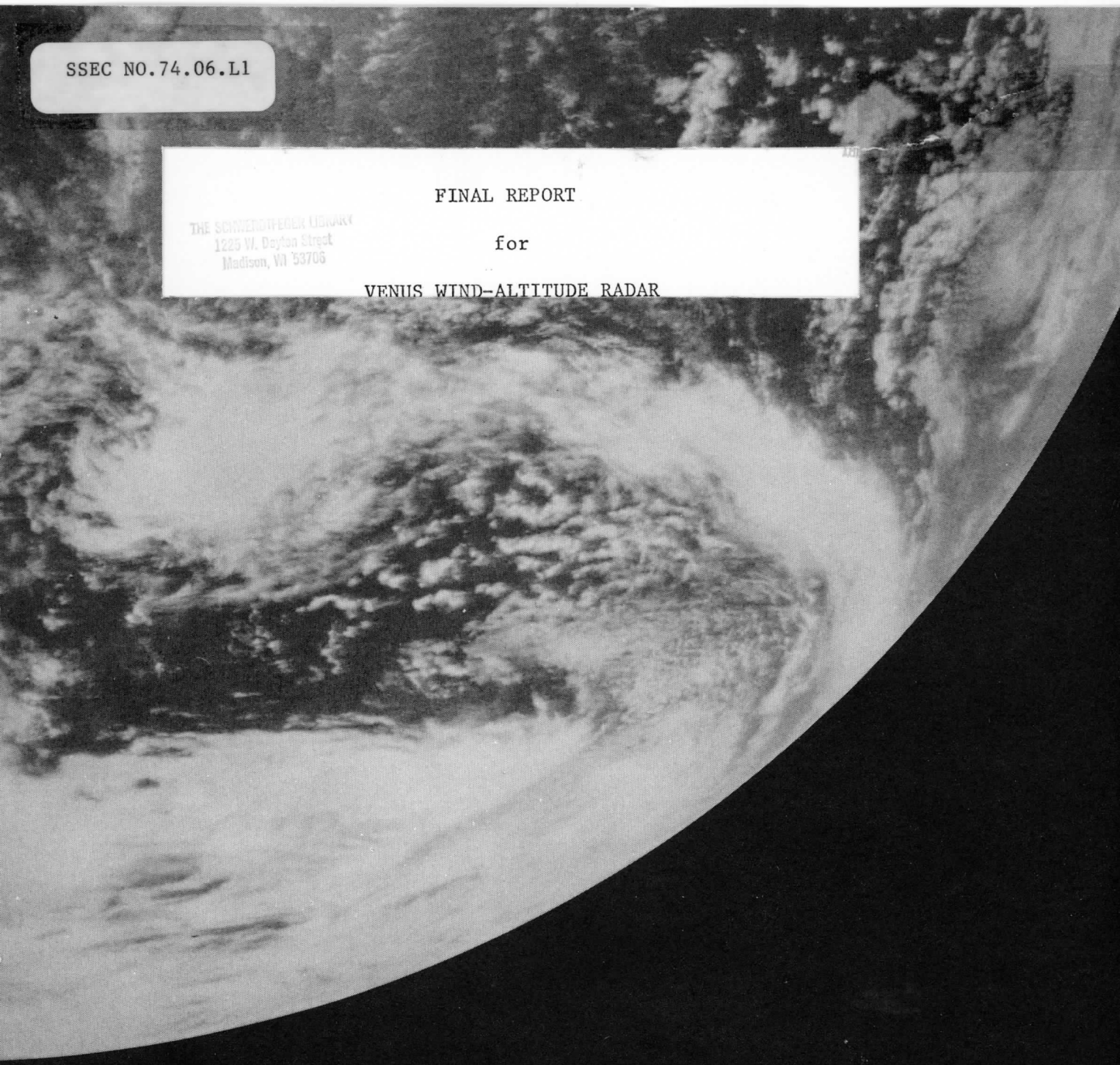

A REPORT

from the space science and engineering center
the university of wisconsin-madison
madison, wisconsin

THE SCHWERDTFEGER LIBRARY
1225 W. Dayton Street
Madison, WI 53706

FINAL REPORT

for

VENUS WIND-ALTITUDE RADAR

(16 January 1974-30 June 1974)

by Nadav Levanon

June 1974

Prepared under Contract No. NAS2-8015 by

The University of Wisconsin
Space Science and Engineering Center
1225 West Dayton Street
Madison, Wisconsin 53706

for

AMES RESEARCH CENTER

NATIONAL AERONAUTICS AND SPACE ADMINISTRATION

INTRODUCTION

This final report briefly summarizes the major technical conclusions of the design study on adding a radar altimeter to the Pioneer Venus small probe.

A detailed summary of the Radar Altimeter Experiment Definition Phase Work appears as an addendum to the University of Wisconsin's proposal for:

> Design, Fabrication, and Test of a Net Flux Radiometer
> for Use on the Pioneer Venus Mission

submitted to NASA on 24 May 1974 in accordance with Contract NAS5-7882.

The highlights of the Radar Altimeter section of this proposal are given in Section 1.

1.0 HIGHLIGHTS OF THE RADAR ALTIMETER (RA) PROPOSAL AS AN ADD-ON TO THE NET FLUX RADIOMETER (NFR)

	NFR	NFR & RA
Cost	$1,233,488	$1,461,658
Weight	475 g	765 g
Power	2.21 W	3.77 W

2.0 RADAR ALTIMETER SYSTEM DESCRIPTION

The radar altimeter is a modification of the balloon borne radar altimeter used on the TWERLE (NIMBUS-F) program, for which more than 500 altimeters have been built. The instrument is basically a delay-lock radar utilizing a superregenerative RF stage as both the receiver and the transmitter. The 400 MHz RF pulses with 0.4 μs pulse-width and a pulse-repetition-rate which varies between 15 KHz and 37.5 KHz.

A delay-lock loop is used to provide a simple range tracking and measuring system, with the pulse repetition rate being (at lock) a measure of the altitude. Small perturbations added to the repetition rate are used to generate a range tracking error signed and have an effect equivalent to the split gate used in conventional tracking radars. The loop bandwidth controls an inherent averaging period.

2.1 Altimeter Functional Description

A block diagram of the radar altimeter is shown in Figure 2-1. The superregenerative RF stage provides a receiving window followed by a transmitted pulse. When the pulse generator gates the RF power oscillator into an oscillatory mode, the presence of signal or noise sets the initial value of the growth of oscillations. The stronger the signal and shorter the delay before the oscillation amplitude reaches the saturation level. The high power oscillations are continued at the saturation level until cutoff by the termination of the gate (quench pulse).

The bias-control loop maintains a constant average width of the RF pulses, despite the tendency of the width to increase in the presence of signal, by adjusting the bias on the RF stage. The detected received signal is extracted from the bias circuit. The superregenerative detector has a logarithmic response as long as it is allowed to reach saturation.

The period of the quench pulses is controlled by the voltage-controlled oscillator (VCO) and is scanned from longer to shorter intervals. As the period coincides with the delay of the return, each receiving window detects the return from a preceding transmitted pulse. It should be noted that the scanning rate is relatively slow; hence an average return pulse is being reconstructed from many returns in a manner similar to the stroboscopic principle of a sampling oscilloscope.

In order to detect the peak of the returned pulse the repetition period is perturbed at a low rate, f_p. This results in a controlled dither in the position of the receiving window relative to the returned pulse. On the leading slope the detected perturbation will be in-phase with the injected perturbation. On the trailing slope the detected perturbation will be out-of-phase with the injected one. The multiplier performs synchronous detection of this perturbation yielding a signal proportional to the derivative of the returning pulse average waveform. The output of the multiplier is an error signal fed to the integrator whose output controls the VCO period. When the receiving window coincides with the peak of the return from a previous pulse, the derivative is zero; hence zero error signal is fed to the integrator and the loop locks. The sense of the error is such that the feedback loop keeps the receiving window aligned with the peak of the return in the locked condition. Dynamics of the loop are similar to those of the well-known phase-lock loop (PLL).

The VCO repetition period at lock T is related to the altitude h by the following equation:

$$h = \frac{c}{2} (NT - \tau) \tag{2.1}$$

where c is the velocity of light, τ is internal delay, and N is the

subharmonic mode number which will be discussed in a later section on range ambiguity. Figure 2-2 is a timing diagram for a first-mode case. This figure shows that the internal delay, τ, is measured between the receiving window and the end of the transmitted pulse, which, when this pulse returns, will be the position of the peak.

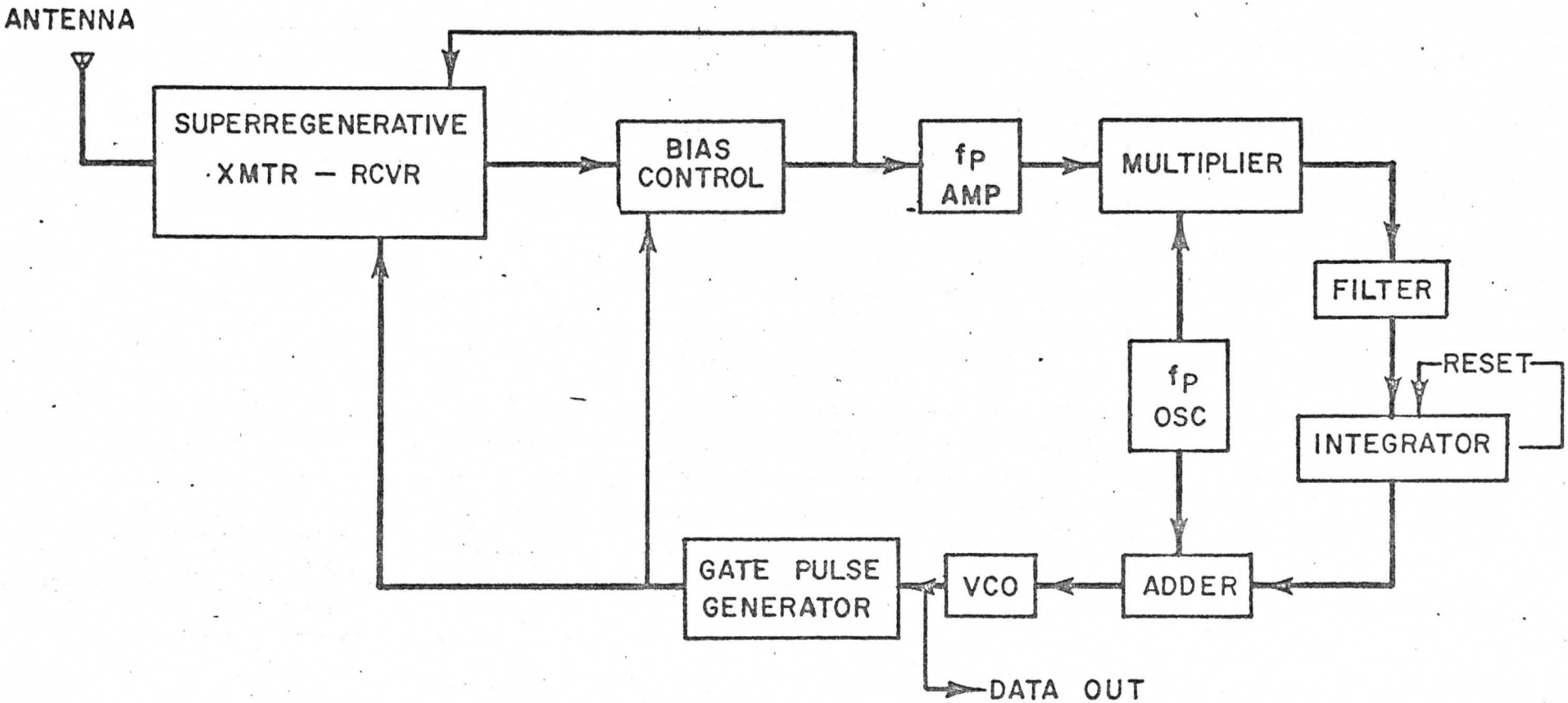

Figure 2-1. Radar Altimeter Block Diagram

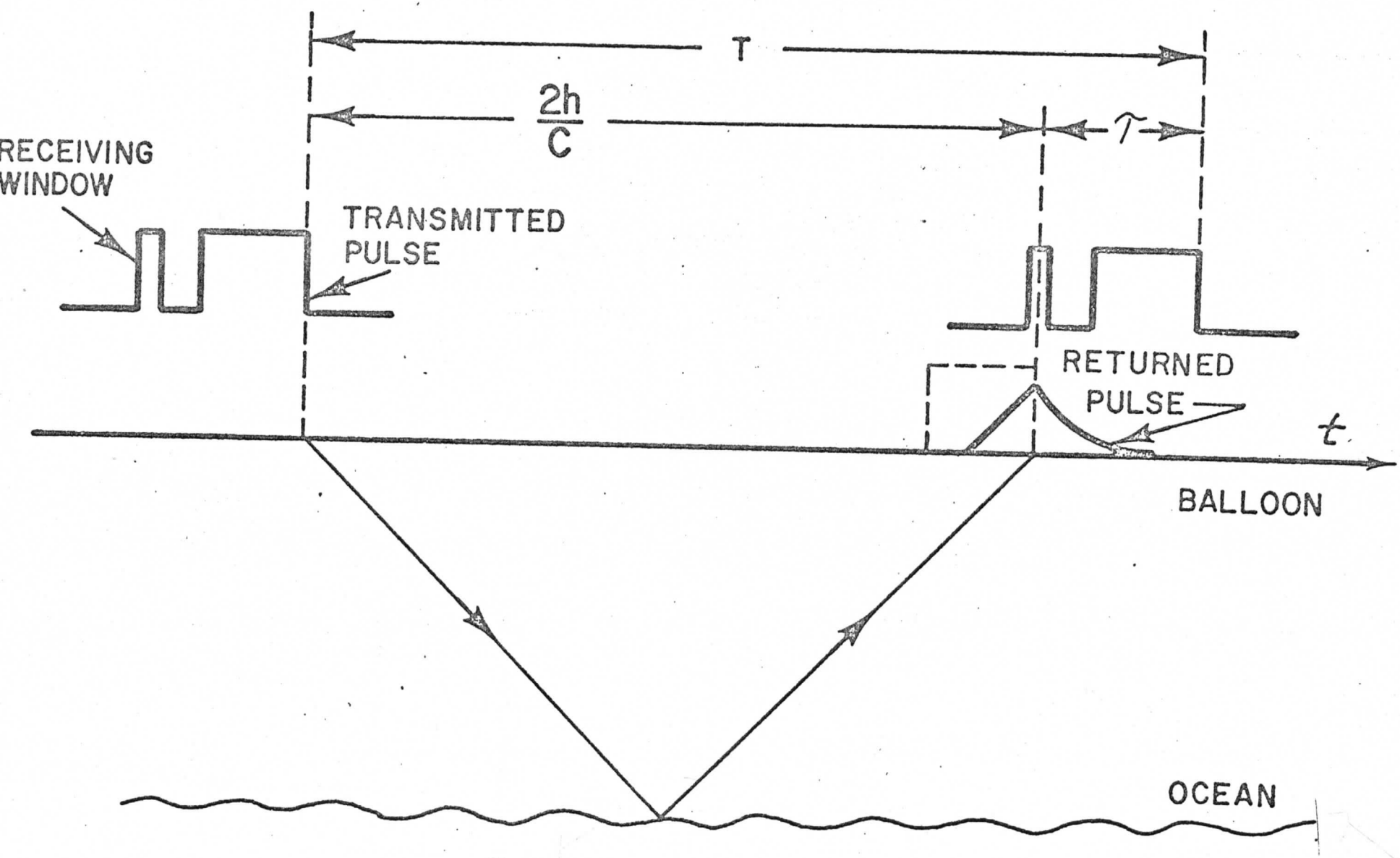

Figure 2-2. Timing Diagram

3.0 VENUS PROBE RADAR ALTIMETER ABMIGUITY, RESOLUTION AND DATA HANDLING LOGIC

3.1 Inherent ambiguity

As indicated in the functional description the altitude h is derived from the pulse repetition period T by the equation

$$h = \frac{C}{2} (NT - \tau) \qquad (3.1)$$

where C is the velocity of light, τ is in internal delay and N is the mode number which is equal to the number of pulses, minus one, transmitted during a round trip delay.

For the Venus descent, it is suggested that the range of the repetition period to be scanned will be between 67 to 27 μs which corresponds to the repetition period of 15 to 37.5 KHz and, assuming the internal delay τ is zero, to altitude reading of 10 to 4 km respectively.

The ambiguity diagram for such a configuration is given in Figure 3.1. Assuming no loss of lock except at the end of reading range, the enhanced pattern will occur. At 66 km the altimeter will lock at mode 7 (the lowest one available), and will remain in this mode down to an altitude of 28 km. There it will jump again to the lowest mode which is mode 3 and will follow it down to 12 km. It will lock in mode 2 down to 8 km, and in mode 1 from 8 to 4 km. Of course, this pattern is not guaranteed since loss of lock may occur in the middle of the delay range. However, the ambiguity will be equal to the reading, and at the worst case will be 4 km. Such an ambiguity is easily resolved from the history of the descent or from other sensors.

3.2 Interface ambiguity

The basic principle of the interface circuitry is given in Figure 3.2. The length of 32768 altimeter repetition periods is measured by counting the 4096 Hz clock. The first "a" stages of the shift register are not read. The remaining "b" stages are read, and 0_v will indicate the number of overflows.

Using (1) and setting τ=o, the altitude h when the reading is n, is given by

$$h = \frac{150\ 10^6\ N\ 2^a\ (n+0_v 2^b)}{32768\ 4096} \qquad (3.2)$$

or

$$h = 1.118\ 2^a\ (Nn+2^b N0_v) \qquad (3.3)$$

The fact that we have a term $N0_v$ which is the altimeter mode number times the counter overflow, (or the inherent ambiguity times the interface ambiguity) means that we will not be able to distinguish between the two, and at low n count the ambiguity may become too small to resolve. In other words, we cannot allow interface ambiguity, i.e., the counter to overflow.

The maximum count is given by

$$\text{count}_{(\max)} = \frac{32768\ 4096}{\text{f alt}_{(\min)}} = \frac{32768\ 4096}{15000} = 8947$$

and

$$2^{13} < 8947 < 2^{14}$$

which means that the counter length has to be

$$a + b = 14 \qquad (3.4)$$

Now we can set $0_v = 0$ in (3) and get

$$h = (1.118\ 2^a N)n \qquad (3.5)$$

The term in brackets is the resolution. For a=0, i.e., all 14 stages of the counter are read out, the resolution will be 1.118 N meters, or, about 8 meters at the beginning of the descent (66 km, N=7) and 1 meter at 4 km (N=1).

Reducing the number of bits below 14 will worsen the resolution by a factor of 2 for each bit removed.

To increase the resolution, both the number of bits and the clock frequency has to be increased by the same factor. An alternative to an increase in the clock frequency could be to increase the gate time by measuring the period of twice (or more) as many altimeter periods. This, however, will

increase the count time from the 2 sec which is the maximum count period in the above scheme.

Since a resolution of 1 to 8 meters is considered sufficient, the altimeter data handling logic was designed for the required 14 bits, utilizing two 8 bit data words. The logic is outlined in the following section and in Figure 3.3. The logic in Figure 3.3 requires 9 IC packages.

The operating sequency of the radar altimeter logic is slaved to the telemetry frame by the action of the two (2) read envelopes. Two 8 bit data words are required to read-out the data accumulated for each sample. A sequence is started when RE(2) occurs. When RE(2) is at a logic 1 level, both the 15 bit counter [Q] and the 14 bit counter [R] are held in a reset state (see Figure 3.3). When RE(2) falls to a logic Ø level the reset is released and the two counters begin accumulating counts. Counter [Q] counts the output of the RA VCO and stops when it has accumulated 2^{15} counts. Counter [R] counts the 4096 Hz system clock and is also stopped by counter [Q] reaching 2^{15} counts. This process takes about 2 seconds.

When RE(1) occurs the 16 bit shift/register [S] is loaded from counter [R] and the first eight bits are shifted out. RE(2) shifts out the last 8 bits and also resets the logic for another sample.

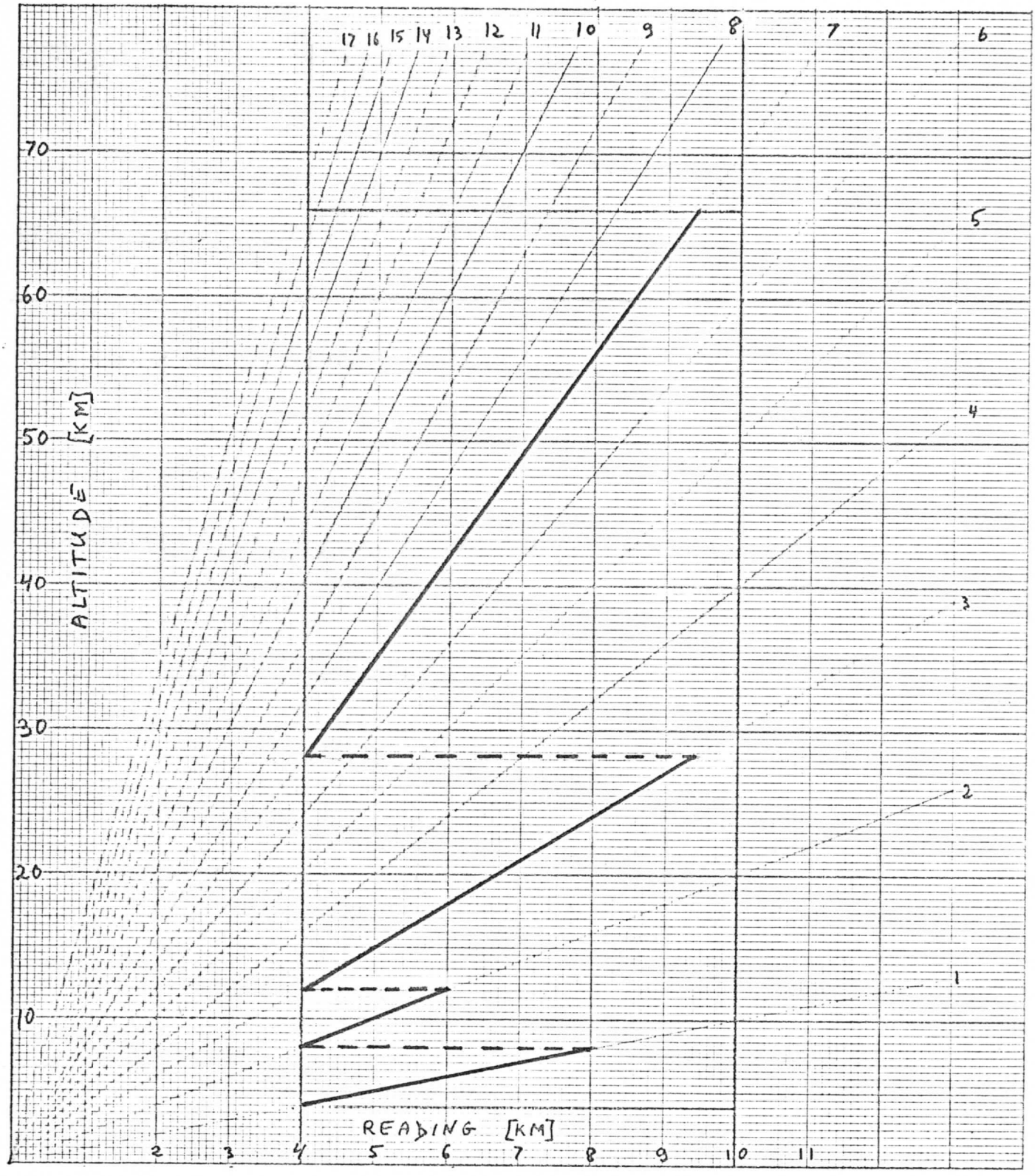

Fig. 3.1. Ambiguity Pattern

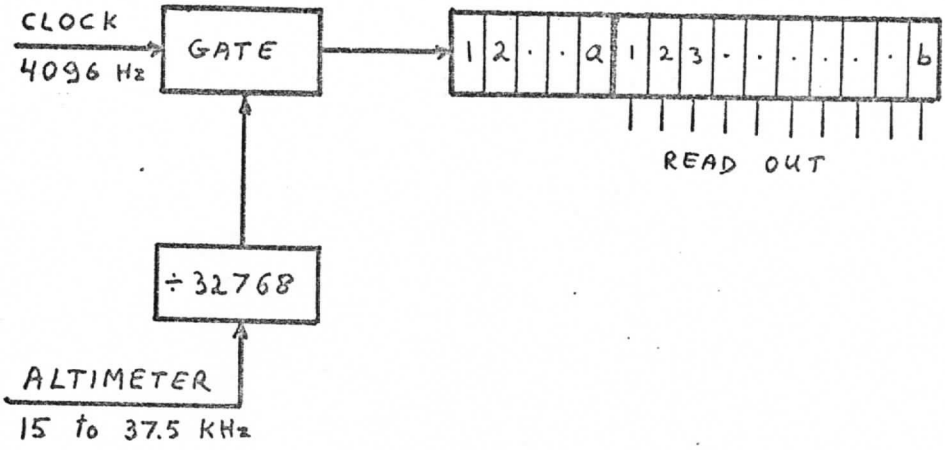

Fig. 3.2. Altimeter Interface

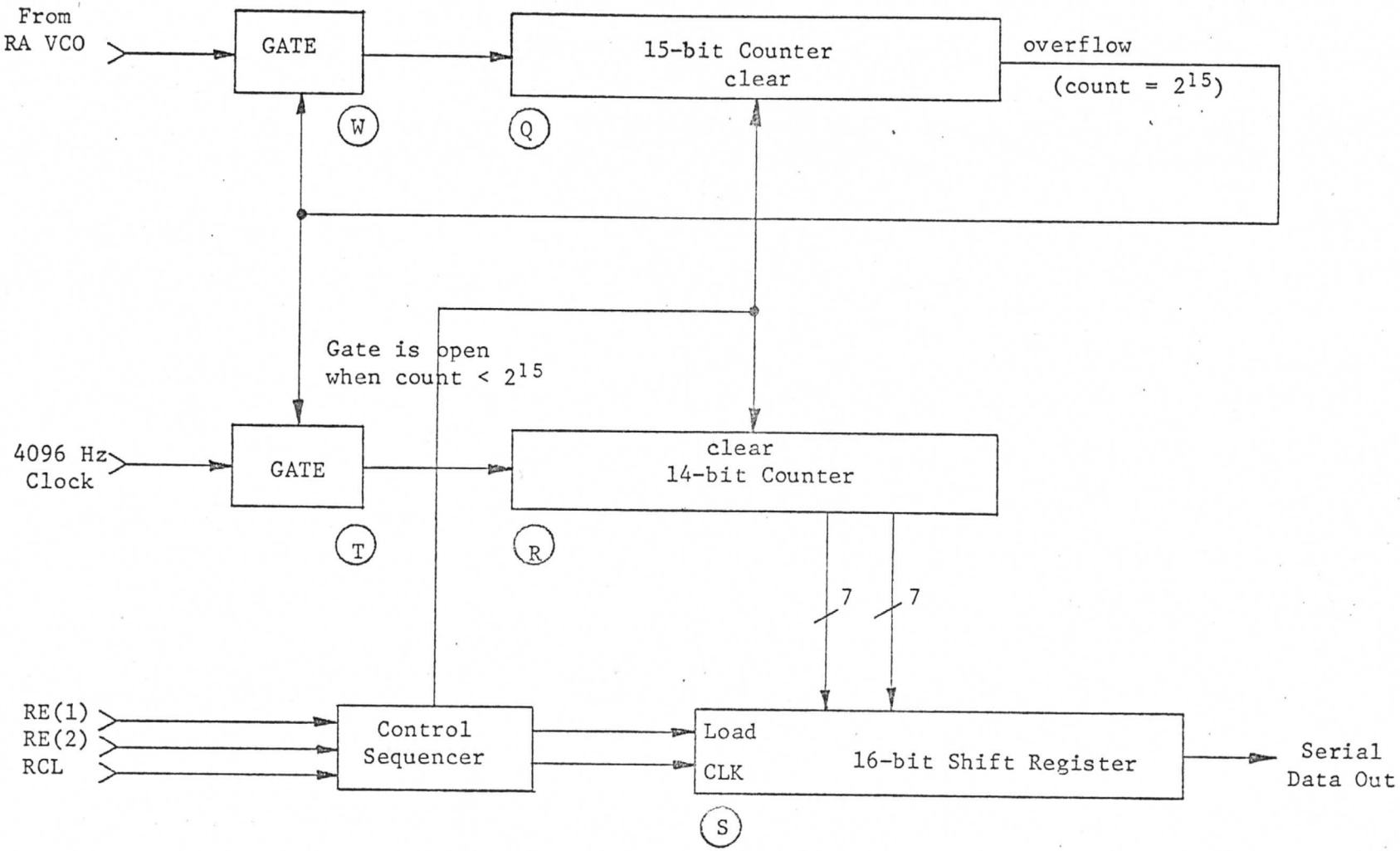

Fig. 3.3. Radar Altimeter Logic Block Diegram

4.0 MODIFIED RF STAGE, RF POWER AND RANGE

4.1 General

The main electrical modification required in order to adapt the TWERLE balloon borne altimeter to the Venus application, was to increase the output RF power of the altimeter without reduction in its sensitivity, in order to achieve a net gain in the acceptable path-loss.

4.2 Selection of RF Transistor and Oscillator Configuration

Various RF transistors were tested and the results are summarized in Table 4.1. CTC transistor type D20-28 was selected. The common collector configuration (Fig. 4.1) was also selected as optimal for this transistor.

4.3 Specifications

The electrical parameters of the complete altimeter are summarized below:

RF frequency	400 MHz
Peak RF Power Output	15 W
RF Pulse Width (-3 dB)	0.4 µs
Sweep Range	25 - 65 µs
Sweep Time	60 s
Quench Pulse	2 µs
Perturbation Width (ptp)	0.4 µs
Loop Bandwidth (@29 µs delay and 129 dB path-loss)	2 Hz
Maximum Path-loss	161 dB
DC Power Input (max)	1.4 W @ +12V ± 10% 56 mA and -12V ± 10% 63 mA

Table 4.1. TEST RESULTS

(All measurements at 24 volts)

Transistor Type	Mode	P_o*** W	P_o*** dBm	S** dBm	Path Loss dB	Expected Altimeter Path Loss dB	ΔF* MHz	Comment
PH0412H	CB	8	39	-81	120	140	2	Low S; very selective
40941	CC	2.5	34	-94	128	148	7	Large ΔF lowers S
D1-28	CC	3.2	35	-96	131	151	3	
C12-28	CB	7	38	-94	132	152	6	C_{eb}=22 pF; Large ΔF
2N5917	CC	3.2	35	-101	136	156	5	Very high S; Large ΔF
2N5108	CC	4	36	-102	138	158	2	High S; Small ΔF
D20-28	CC	16	42	-99	141	161	--	High P_o, Good S, Small ΔF
TWERLE Altimeter (2N5108)	CC	1.6	32	-97	129	149	2	149 dB actual measured path loss for Altimeter locking

* ΔF is the difference between the transmitted frequency and the most sensitive receiving frequency.

**S (sensitivity = 20 dB above loss-of-lock) is measured at the transmitted frequency.

***P_o is the rms value of the pulse RF power

Notes: (1) Both modes were tested for all types. Only the better mode is shown.

(2) C_{eb} is necessary for the higher power transistors to obtain the rated power output. However, C_{eb} tends to increase ΔF. In most cases, C_{eb} has an optimum value which results in a small ΔF, and power output slightly below the maximum attainable.

(3) Types C25-28 and C40-28 were also tested but performed very poorly.

4.4 Range Estimate

The expected range from the altimeter is shown in Figure 4.2. The expected path loss in the Venus descent ranges from 145 dB at an altitude of 65 km to 120 dB at an altitude of 10 km, assuming probe antenna with 5 dB gain over isotropic. The measured path loss in which a 15 W altimeter will lose lock is 161 dB. This measurement is performed in the lab with a microwave acoustic delay line. The margin between the lab-simulated loss-of-lock line, and the expected path loss at 65 km (the beginning of the descent) is 16 dB. For comparison, in the TWERLE balloon flight at 15 km over the ocean, the expected path loss is 109 dB. The production line of the TWERLE altimeters will pass any altimeter yielding at least 125 dB path-loss measured with the same microwave acoustic delay line. Hence the same margin of 16 dB. It should be mentioned however that the typical TWERLE altimeter path-loss is 135 dB, with the best ones achieving 150 dB.

REVISIONS			
LTR.	DESCRIPTION	DATE	APPROVED

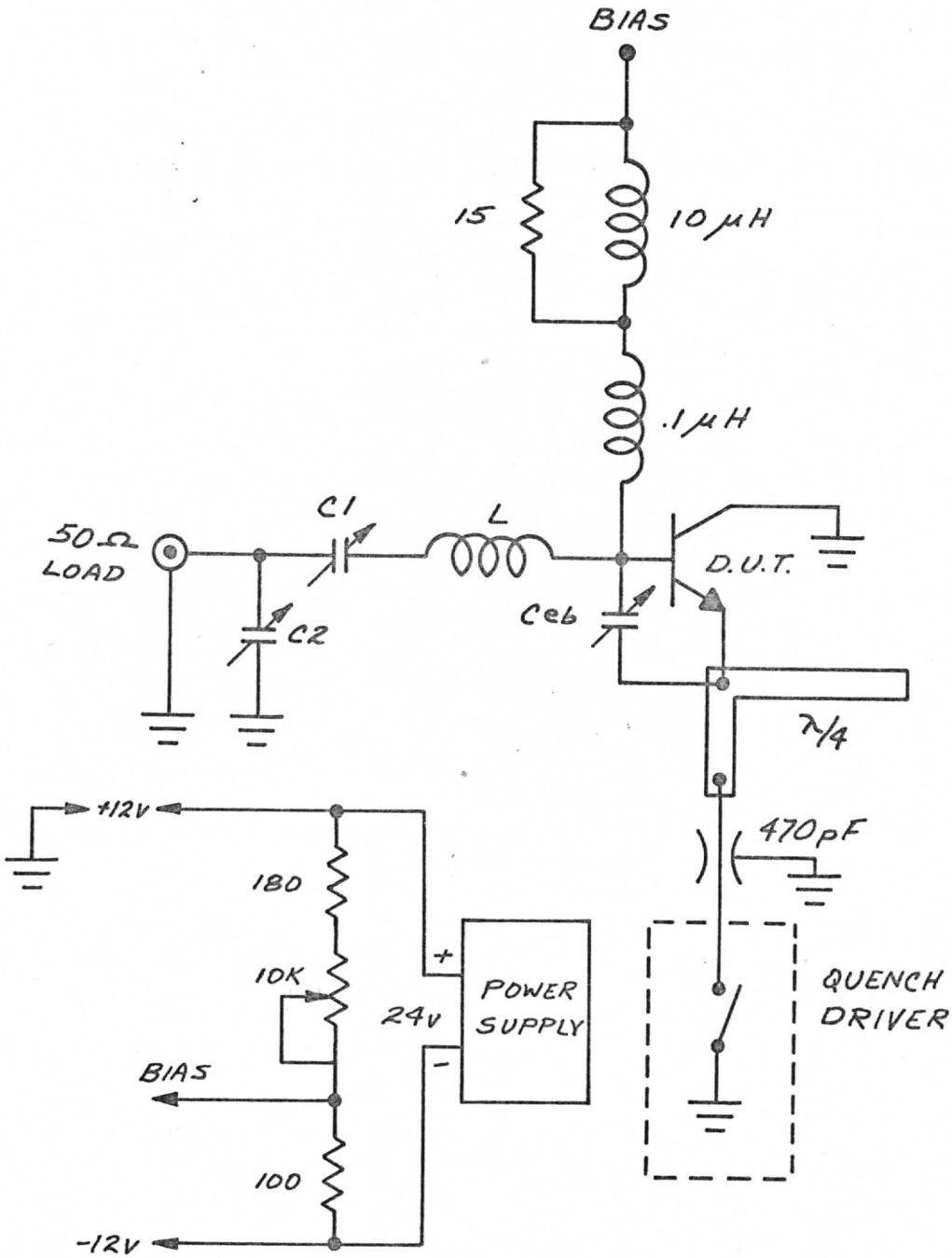

THE UNIVERSITY OF WISCONSIN
SPACE SCIENCE & ENGINEERING CENTER
MADISON, WISCONSIN

TITLE

Fig. 4.1. Common collector oscillator

SCALE	DRAFTSMAN DATE	CHECKER DATE	ENGINEER DATE
NEXT HIGHER ASSEMBLY	PRODUCT ASSURANCE DATE	PROJECT APPROVAL DATE	
PROJECT NO. / SIZE	SHEET OF	DRAWING NO.	

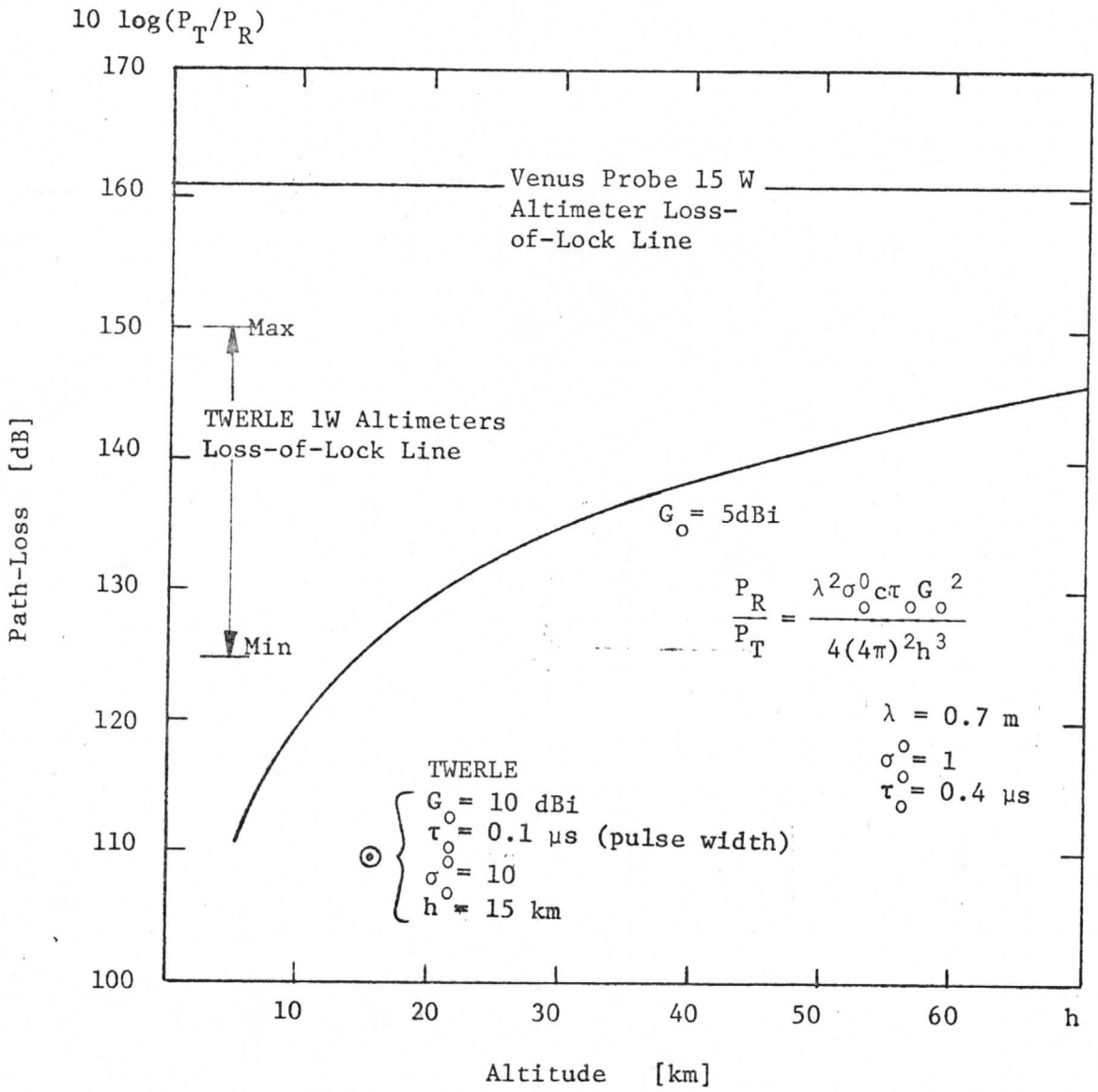

Figure 4.2. Radar Altimeter Path-loss Versus Altitude

5.0 ANTENNA

5.1 Antenna Electrical Design

The proposed antenna for the radar altimeter on board the small Venus probe is an array of two $\lambda/4$ monopoles, diametrically opposed around the edge of the probe cone. Each monopole has a parasitic element. The parasitic element serves to improve the front-to-back ratio. The parasitic element is parallel to the driven element and has essentially the same length.

A photograph of a real size probe with the proposed antenna is given in Figure 5.1.

5.2 Theoretical Pattern

A simplified E-plane theoretical pattern of the antenna could be obtained using the following assumptions:

a. Each monopole above the cone surface behaves like a short element above a ground plane, whose E-plane pattern is given by $\cos\theta$, where θ is measured from the line perpendicular to the element.

b. The two monopoles (with their respective reflections) comprise a two element collinear array. This array factor is given by:

$$|AF_1| = \frac{1}{2} \frac{\sin \psi_1}{\sin \frac{\psi_1}{2}} \tag{5.1}$$

where

$$\psi_1 = 2\pi \frac{d_1}{\lambda} \sin\theta \tag{5.2}$$

and d_1 is the effective element spacing (found experimentally to be 15% longer than the actual spacing).

c. The parasitic element provides a second array factor, given by

$$|AF_2| = 1 + \left|\frac{I_2}{I_1}\right| e^{j(\psi_2 - 2\pi \frac{d_2}{\lambda} \cos\theta)} \tag{5.3}$$

where I_2 are the currents into the driven element and parasitic element

respectively, ψ_2 is the lead of I_2 over I_1, and d_2 is the spacing between the driven element and parasitic element. (In eq. 5.3, $\theta = 0$ on the side of the driven element.)

The theoretical E-plane pattern is hence given by:

$$|E_{(\theta)}| = \cos\theta \cdot \frac{1}{2} \frac{\sin\left(2\pi\frac{d_1}{\lambda}\sin\theta\right)}{\sin\left(\pi\frac{d_1}{\lambda}\sin\theta\right)} \left[1 + \left|\frac{I_2}{I_1}\right| e^{j\left(\psi_2 - 2\pi\frac{d_2}{\lambda}\cos\theta\right)}\right] \quad (5.4)$$

5.3 Measured Pattern and Gain

In Figure 5.2 the theoretical pattern is plotted together with a measured pattern. The measured pattern was taken with the ÷25 scaled down model (Fig. 5.3) in a 10 GHz antenna range. The parameters used for the theoretical pattern are:

$$d_1 = 1.18\ \lambda$$

$$\left|\frac{I_2}{I_1}\right| = 0.78$$

$$d_2 = 0.0638\ \lambda$$

Area integration of the patterns yielded gains (based on E-plane only) of 7.2 dBi for the theoretical pattern, and 5.95 dBi for the measured pattern. Fig. 5.4 is a pattern measured with real size probe model.

5.4 Antenna Mechanical Design

Two identical antenna assemblies will be provided for each small probe. Both will be mounted outside the pressure vessel and will be deployed on command from a stowed position. The antenna assemblies will be electrically interconnected via a co-axial line which passes through the shell wall and will interface with an electronics module within the pressure shell. The outboard segment of the co-axial line will be flexible to permit rotation of the antennas during deployment.

When fully deployed, the antenna elements will be diametrically opposed with maximum separation from other deployed assemblies. The antenna tips will extend approximately 19 cm beyond the aeroshell.

All four antenna elements will be identical, and will be designed to provide maximum stiffness and minimum weight. Tubular configuration is proposed to satisfy both of these requirements.

A structural substrate of Inconel will have an external coating of electrodeposited gold for improved electrical conductivity. A coating thickness of 0.0002 inch provides sufficient skin depth at 400 MHz.

Although the density of Inconel alloy 718 is high, its yield-strength/weight ratio at 500°C exceeds that of exotic aerospace materials such as titanium or beryllium. In addition, it is resistant to the corrosive Venus atmosphere without special surface treatment.

The reflective element will be spring-loaded against the active element as shown in Fig. 5.6 to permit a separation of 45° in the deployed position. A simple detent assembly will lock the reflector at the required angle.

At deployment the platform will rotate the assembly to the proper position while the reflector is simultaneously separating from the active element.

A co-axial conductor connects each antenna array to the electronics module. Key elements of the co-axial line are a leak-tight penetration through the pressure shell and a short flexible section to permit rotation during deployment.

A commercially available co-axial conductor manufactured by Advanced Cable Systems Inc. is rated for operation above 500°C and appears to satisfy the mission requirements.

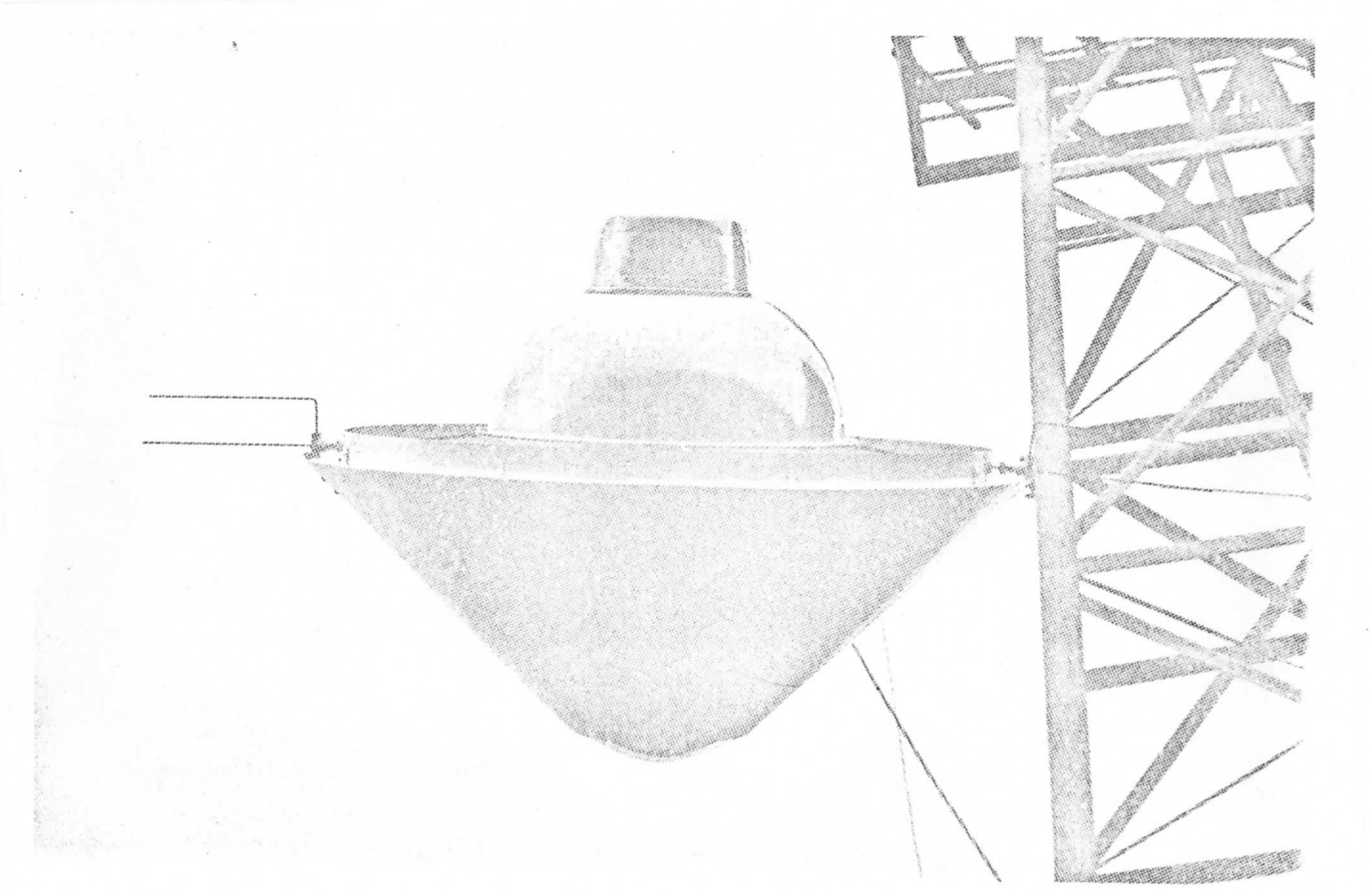

Fig. 5-1 A real size probe model with the proposed altimeter antenna

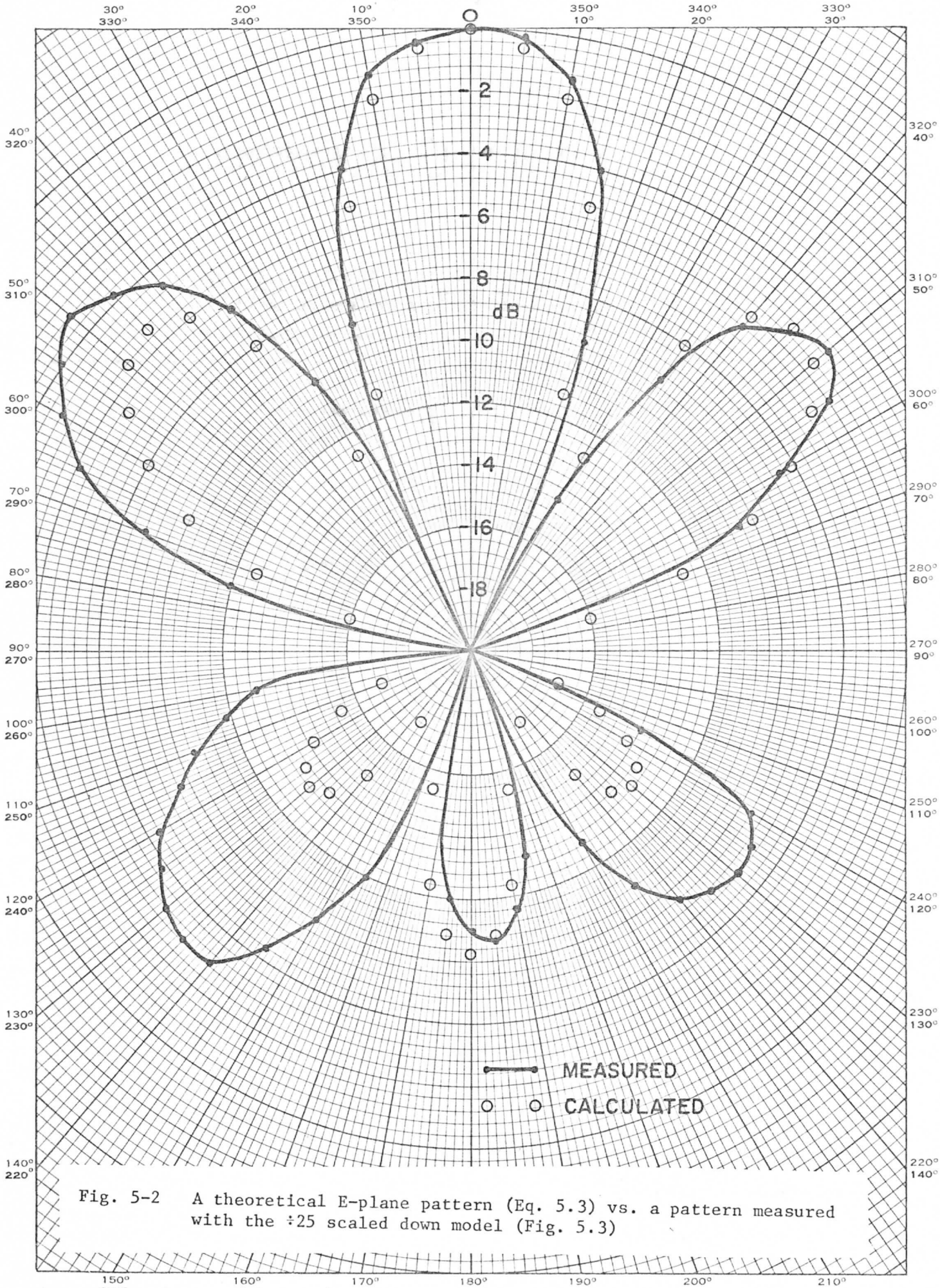

Fig. 5-2 A theoretical E-plane pattern (Eq. 5.3) vs. a pattern measured with the ÷25 scaled down model (Fig. 5.3)

Fig. 5-3 A ÷25 scaled down model as used in a 10 GHz antenna range

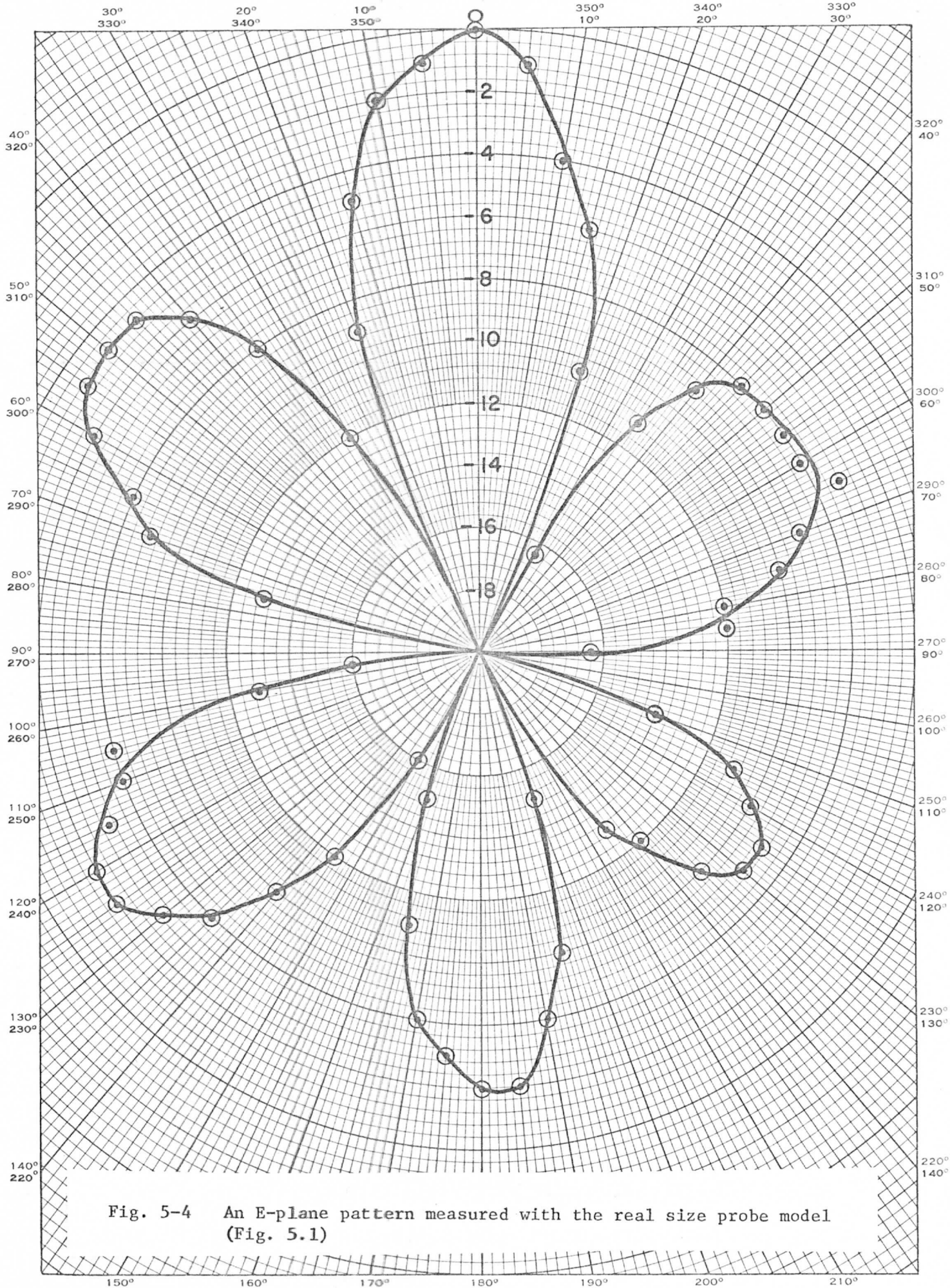

Fig. 5-4 An E-plane pattern measured with the real size probe model (Fig. 5.1)